

Luminescence properties of dysprosium doped barium aluminosilicate phosphors prepared by the solid state reaction method

Ishwar Prasad Sahu¹

Received: 27 June 2016 / Accepted: 28 July 2016 / Published online: 4 August 2016
© Springer Science+Business Media New York 2016

Abstract A series of $\text{BaAl}_2\text{Si}_2\text{O}_8:x\text{Dy}^{3+}$ ($x = 1.0, 1.5, 2.0, 2.5$ and 3.0 mol%) phosphors were prepared by the solid state reaction method. Crystal structures of the sintered phosphors were hexagonal structure with space group of $P6/mmm$. The chemical composition of the sintered $\text{BaAl}_2\text{Si}_2\text{O}_8:\text{Dy}^{3+}$ (2.0 %) phosphor was confirmed by the energy dispersive X-ray spectroscopy. Thermoluminescence kinetic parameters of discussed $\text{BaAl}_2\text{Si}_2\text{O}_8:x\text{Dy}^{3+}$ phosphors were calculated by peak shape method. Under the ultraviolet excitation, emission spectra of $\text{BaAl}_2\text{Si}_2\text{O}_8:x\text{Dy}^{3+}$ phosphors were composed of broad band with the characteristic emission of Dy^{3+} ions are peaking at 478 nm (blue) and 575 nm (yellow), originating from the transitions of ${}^4\text{F}_{9/2} \rightarrow {}^6\text{H}_j$ state (where $j = 15/2, 13/2$). Commission Internationale de L'Eclairage coordinates has been calculated for each sample and overall emission is near white light. The possible mechanisms of discussed white light emitting phosphors were also investigated. In order to investigate the suitability of the phosphors as white color light sources for industrial uses, color purity, correlated color temperature (CCT) and color rendering index (CRI) were calculated. Values of color purity, CCT, CRI were found, well within the defined acceptable range. The peak of mechanoluminescence intensity increases linearly with increasing impact velocity of the moving piston, which suggests that sintered phosphors, can be used as sensors to detect the stress of an object.

1 Introduction

Generally speaking, white lighting phosphors were obtained by combination of the currently available blue, green and red phosphors [1]. However, it is difficult to fabricate such a phosphor that retain the persistent color as white all the time, the reason is that different phosphors seldom have very similar decay ratios to ensure the white color constant [2]. These problems can be overcome by using a single phosphor that emits simultaneously blue, green/yellow and red light whose combination constitutes white emission via the combination of emission in different colors from one kind of luminescence center [3, 4]. A more promising approach is to find such a material that can produce white emission via the combination of emission in different colors from one kind of luminescence center. In recent years, barium aluminosilicate compounds are a good type of promising host materials due to its special properties, such as low cost, easy preparation, excellent thermal and chemical stabilities, and especially the strong absorption in the ultra-violet (UV) [5].

Luminescence properties of Eu^{2+} activated $\text{MAl}_2\text{Si}_2\text{O}_8$ ($\text{M} = \text{Ca}, \text{Sr}, \text{Ba}$) phosphors, which show stable phases prepared by solid state reaction was reported by Clabau et al. [6]. Fluorescence and phosphorescence properties of the low temperature forms of the $\text{MAl}_2\text{Si}_2\text{O}_8:\text{Eu}^{2+}$ ($\text{M} = \text{Ca}, \text{Sr}$ and Ba) compounds was reported by Clabau and Zhang et al. [7] reduced from Eu^{3+} to Eu^{2+} in $\text{MAl}_2\text{Si}_2\text{O}_8$ ($\text{M} = \text{Ca}, \text{Sr}$ and Ba) in air condition by Cui-miao. Recently, $\text{Ba}_2\text{MgSi}_2\text{Al}_x\text{O}_7$ host used for white light emitting diodes by doping Eu^{2+} , Mn^{2+} [8, 9]. After that, Ma et al. [10] studied the effect of Sr^{2+} doping on structure and luminescence properties of $\text{BaAl}_2\text{Si}_2\text{O}_8:\text{Eu}^{2+}$ phosphor and Pawade and Dhoble [11] studied trap depth and Dy^{3+} luminescence in $\text{BaAl}_2\text{Si}_2\text{O}_8$ phosphor. Rare earth (Eu^{2+} ,

✉ Ishwar Prasad Sahu
ishwarprasad1986@gmail.com

¹ School of Studies in Physics and Astrophysics, Pt. Ravishankar Shukla University, Raipur, C.G. 492010, India

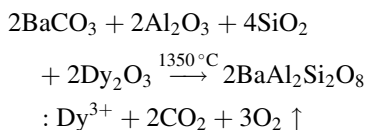
Ce³⁺) activated BaAl₂Si₂O₈ blue emitting phosphor was reported by Pawade et al. [12]. pure hexagonal and monoclinic Sm²⁺/Sm³⁺ co-doped BaAl₂Si₂O₈ phase using a simple sol–gel technique was reported by Lia et al. [13] and studied photoluminescence properties. Previous studies indicate that the BaAl₂Si₂O₈ compound is a good type of promising host materials for rare earth ions doped phosphor. However, to the best of our knowledge, the photoluminescence properties of BaAl₂Si₂O₈:Dy³⁺ phosphors have not been reported yet.

In this article, to find a white light for solid state lighting, a series of BaAl₂Si₂O₈:x Dy³⁺ ($x = 1.0, 1.5, 2.0, 2.5$ and 3.0 mol%) phosphors were synthesized by solid state reaction method and found the samples have white light emission. The crystal structure, particle size, surface morphology, chemical composition and different stretching modes were analyzed by X-ray diffractometer (XRD), transmission electron microscopy (TEM), field emission scanning electron microscopy (FESEM) coupled with energy dispersive X-ray spectroscopy (EDS) and fourier transform infrared (FTIR) spectra respectively. The luminescence properties were also investigated on the basis of thermoluminescence (TL) photoluminescence (PL), decay, mechanoluminescence (ML) and ML decay.

2 Experimental

2.1 Phosphor preparation

The series of dysprosium doped barium alumino-silicate namely BaAl₂Si₂O₈:x Dy³⁺ ($x = 1.0, 1.5, 2.0, 2.5$ and 3.0 mol%) phosphors were synthesized by traditional high temperature solid state reaction method. The starting materials were barium carbonate [BaCO₃ (99.90 %)], aluminium oxide [Al₂O₃ (99.90 %)], silicon di-oxide [SiO₂ (99.99 %)], and dysprosium oxide [Dy₂O₃ (99.99 %)], all of analytical grade (A.R.), employed in this experiment. Boric acid (H₃BO₃) was added as flux. Initially, the raw materials were weighed according to the nominal compositions of BaAl₂Si₂O₈:x Dy³⁺ phosphors, then the powders were mixed and milled thoroughly for 2 h using agate mortar and pestle. The chemical reaction used for stoichiometric calculation is:



The ground samples were placed in an alumina crucible and subsequently fired at 1350 °C for 3 h in an air. At last the nominal compounds were obtained after the cooling down of programmable furnace and products were finally ground into powder for characterizing the phosphors.

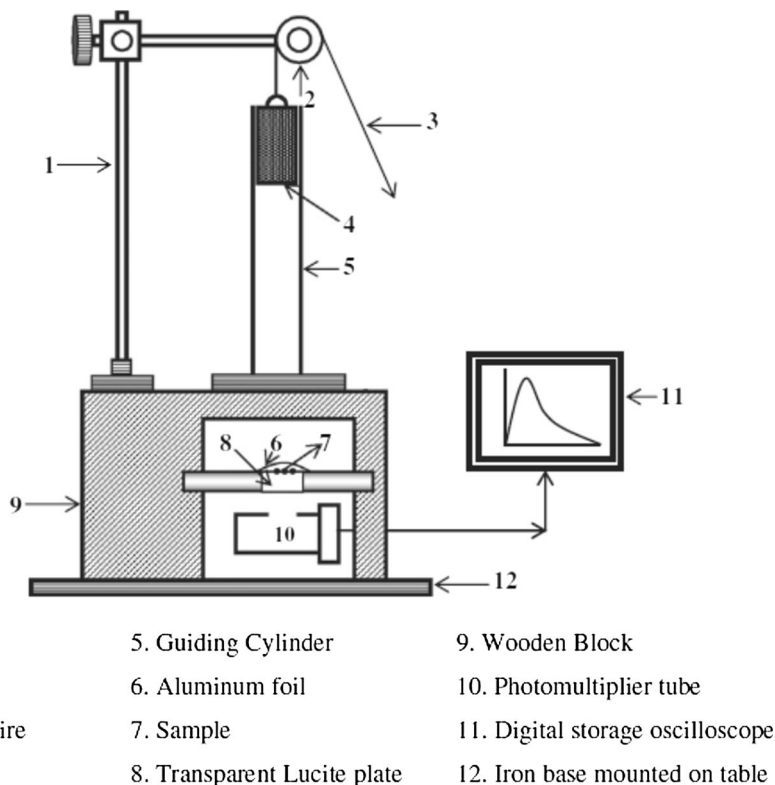
2.2 Measurement techniques

Powder XRD pattern of the prepared BaAl₂Si₂O₈:x Dy³⁺ phosphors has been obtained from Bruker D8 advanced X-ray powder diffractometer using CuKα (1.54060 Å) radiation and the data were collected over the 2θ range 10–80°. Particle size of prepared BaAl₂Si₂O₈:Dy³⁺ (2.0 %) phosphor was determined by TEM using TECHNAI G2 by FEI. The sample required for TEM analysis was prepared by dispersing the prepared BaAl₂Si₂O₈:Dy³⁺ (2.0 %) phosphor in methanol using an ultrasound bath technique. Drop of this dispersed suspension was put onto 200-mesh carbon coated copper grid and then dried into an air. The surface morphological images of prepared BaAl₂Si₂O₈:Dy³⁺ (2.0 %) phosphor was collected by the FESEM. The samples were coated with a thin layer of gold (Au) and then the surface morphology of prepared phosphor were observed by the FESEM; ZIESS Ulta Plus-55, operated at the acceleration voltage of 20 kV. An EDX spectrum was used for the elemental (qualitative and quantitative) analysis of the prepared phosphor. FTIR spectra were recorded in the middle infrared region (4000–400 cm⁻¹) with the help of IR Vertex-70 by Bruker. For investigating the functional groups (4000–1400 cm⁻¹) and finger print region (1400–400 cm⁻¹) of FTIR spectra, potassium bromide (KBr, IR grade) were mixed with prepared BaAl₂Si₂O₈:Dy³⁺ (2.0 %) phosphor. TL glow curves were recorded with the help of TLD reader 1009I by Nucleonix (Hyderabad, India Pvt. Ltd.). For the TL measurement, the quantities of the powder samples were kept fixed (8 mg). The excitation and emission spectra were recorded on a spectrofluorophotometer, Shimadzu (RF 5301-PC) using the Xenon lamp (150 W) as excitation source when measuring. The decay curves were obtained using a Perkin Elmer fluorescent spectrometer with the proper excitation under a UV lamp. All measurements were carried out at the room temperature.

2.3 Experimental setup for mechanoluminescence (ML) measurement

The experimental set up used for the impulsive deformation of ML was shown in Fig. 1. A moving piston (load) of particular mass (400 g) and shape (cylindrical) was dropped from different heights for striking the prepared BaAl₂Si₂O₈:Dy³⁺ (2.0 %) phosphor at different impact velocities. The phosphor under study was placed on the upper surface of a transparent lucite plate and it was then covered with a thin aluminum foil and fixed with adhesive tape. The foil reflects light and prevents scattering of the fragments during the impact of a moving piston onto the prepared phosphor. This arrangement eliminates the error in the ML measurement due to the scattering of the

Fig. 1 Schematic diagram of the experimental setup for ML measurement



crystallite fragments during the impact of the load onto the phosphor. The housing is made up of thick soft iron to provide shielding from light and magnetic field. The slit arrangement at the window is provided to adjust the size of the window according to the incident beam. When the prepared phosphor placed on the lucite plate was crushed by impact of the load, light is emitted [14].

By changing the distance between the piston to be dropped and the sample placed on the lucite plate, the impact velocity (v_0) of the load could be changed from 98 cm/s to 328 cm/s, since the pulley and the guiding cylinder used were of negligible friction, the impact velocity (v_0) was taken as $\sqrt{2gh}$, where “g” is the acceleration due to gravity and “h” is the height through which the load is dropped freely. An RCA 931A photomultiplier tube (PMT) was placed below the transparent lucite plate [15]. The PMT was run at 750 V. The output of PMT was connected to the phosphorescent screen oscilloscope (Scientific 300 MHz, SM 340). The ML glow curve can be plotted with the help of SM-340 application software installed in a computer attached with the storage oscilloscope. Care was taken that, except some specific studies, each phosphor sample should have the same mass; therefore, the mass of each sample was measured using a chemical balance. Furthermore, the samples were distributed in a particular area on the lucite plate. The response time of a PMT system was nearly 5 μ s. The error found in the ML measurement was $\pm 5\%$ [16].

3 Results and discussion

3.1 XRD analysis

In order to determine the crystal structure, powder XRD analysis has been carried out. The typical XRD patterns of $\text{BaAl}_2\text{Si}_2\text{O}_8$ and $\text{BaAl}_2\text{Si}_2\text{O}_8:x\text{Dy}^{3+}$ ($x = 1.0, 1.5, 2.0, 2.5$ and 3.0 mol%) phosphors with the standard XRD pattern is shown in Fig. 2a. The position and intensity of diffraction peaks of the prepared $\text{BaAl}_2\text{Si}_2\text{O}_8$ and $\text{BaAl}_2\text{Si}_2\text{O}_8:x\text{Dy}^{3+}$ phosphor were matched and found to be consistent with Joint Committee Powder Diffraction Standard data (JCPDS) file (JCPDS:77-0185) [17], indicating that doping of Dy^{3+} ions does not cause any significant change in the host structure. A comparison of the data with the standard JCPDS file reveals that the diffraction peaks of the $\text{BaAl}_2\text{Si}_2\text{O}_8:x\text{Dy}^{3+}$ phosphors match with those of the standard hexagonal phase with the space group of $P6/mmm$ (191). The atomic parameters of $\text{BaAl}_2\text{Si}_2\text{O}_8$ phosphor was shown in Table 1.

Based on Pauli theory and the effective ionic radius of cations, it was deduced that Dy^{3+} should be expected to occupy the Ba^{2+} sites preferably, since the ionic radius of Dy^{3+} (0.99 Å) is close to that of Ba^{2+} (1.42 Å) compared with the ionic radii of Al^{3+} (0.57 Å) and Si^{4+} (0.41 Å). Figure 2b shows crystal structures and the coordination polyhedral of Dy^{3+} (or Ba^{2+}) ions surrounded by O^{2-} ions for $\text{BaAl}_2\text{Si}_2\text{O}_8:x\text{Dy}^{3+}$. The lattice parameters of the

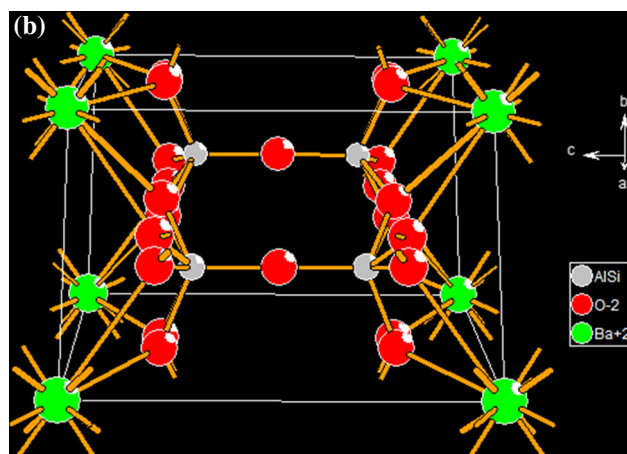
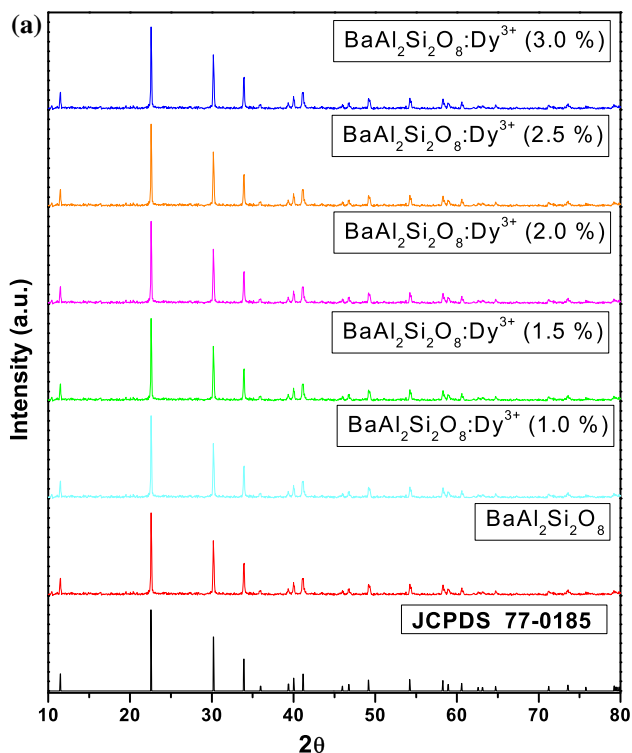


Fig. 2 **a** XRD patterns of $\text{BaAl}_2\text{Si}_2\text{O}_8$ and $\text{BaAl}_2\text{Si}_2\text{O}_8:\text{Dy}^{3+}$ phosphors with different Dy^{3+} concentration. **b** Crystal structure and cation polyhedral arrangements of polymorph $\text{BaAl}_2\text{Si}_2\text{O}_8:\text{Dy}^{3+}$ (2.0 %) phosphor

Table 1 Atomic parameters of $\text{BaAl}_2\text{Si}_2\text{O}_8:\text{Dy}^{3+}$ (2.0 %) phosphor

Atom	Ox.	Wyck.	Site	S.O.F.	x/a	y/b	z/c
Al1	3	4h	3m.	0.5	1/3	2/3	0.28800
O2	-2	12n	..m	0.5	0.45000	0	0.20900
Ba1	2	1a	6/mmm		0	0	0
O1	-2	2d	-6m2		1/3	2/3	1/2
Si1	4	4h	3m.	0.5	1/3	2/3	0.28800

optimum $\text{BaAl}_2\text{Si}_2\text{O}_8:\text{Dy}^{3+}$ (2.0 %) phosphor was calculated using Celref V3. The refined values of hexagonal dysprosium doped barium aluminosilicate were found as; $a = b = 5.2927 \text{ \AA}$, and $c = 7.7883 \text{ \AA}$, $c/a = 1.47171$, $\alpha = 90^\circ$, $\beta = 90^\circ$, $\gamma = 120^\circ$ and cell volume (V) = 187.00 (\AA^3), $Z = 1$, is nearly same [$a = b = 5.2930 \text{ \AA}$, and $c = 7.7900 \text{ \AA}$, $c/a = 1.47175$, $\alpha = 90^\circ$, $\beta = 90^\circ$, $\gamma = 120^\circ$ and cell volume = 189.00 (\AA^3), $Z = 1$], with the standard lattice parameters which again signifies the proper preparation of the discussed $\text{BaAl}_2\text{Si}_2\text{O}_8:\text{Dy}^{3+}$ (2.0 %) phosphor.

3.2 Transmission electron microscopy (TEM)

The particle size of $\text{BaAl}_2\text{Si}_2\text{O}_8:\text{Dy}^{3+}$ (2.0 %) phosphor was displayed in Fig. 3. From the TEM image, it can be observed that the prepared sample consists of particles with different size distribution. The TEM study indicates that the particle size of prepared $\text{BaAl}_2\text{Si}_2\text{O}_8:\text{Dy}^{3+}$ (2.0 %) phosphor was in micrometer range. Moreover, the agglomeration of powder particles was also observed due to the high temperature synthesis.

3.3 Field emission scanning electron microscopy (FESEM)

FESEM studies were carried out to obtain information about surface morphology, grain size, and shape of the synthesized phosphor. The morphologies of prepared $\text{BaAl}_2\text{Si}_2\text{O}_8:\text{Dy}^{3+}$ (2.0 %) phosphor were also observed by means of FESEM in Fig. 4a, b with different magnification. The surface of the $\text{BaAl}_2\text{Si}_2\text{O}_8:\text{Dy}^{3+}$ (2.0 %) phosphor has shown irregular which means the distribution of the crystallite sizes is not homogeneous. The morphological images of prepared $\text{BaAl}_2\text{Si}_2\text{O}_8:\text{Dy}^{3+}$ (2.0 %) phosphor

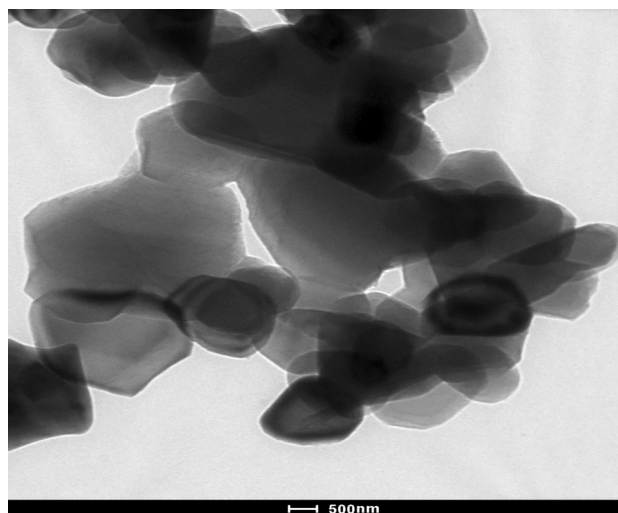


Fig. 3 TEM images of $\text{BaAl}_2\text{Si}_2\text{O}_8:\text{Dy}^{3+}$ (2.0 %) phosphor

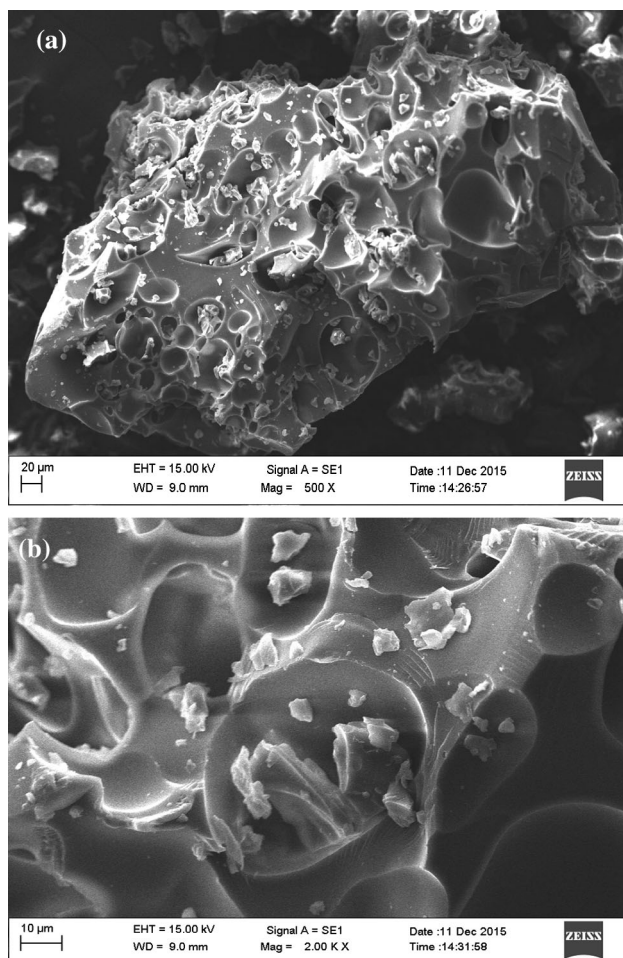


Fig. 4 a, b FESEM image of $\text{BaAl}_2\text{Si}_2\text{O}_8:\text{Dy}^{3+}$ (2.0 %) phosphor with different magnification

displays that the particles are aggregated tightly with each other due to the high temperature synthesis method. From the FESEM image, it can be observed that the prepared sample consists of particles with different size distribution.

3.4 Energy dispersive X-ray spectroscopy (EDS)

Figure 5 shows an EDS spectrum of $\text{BaAl}_2\text{Si}_2\text{O}_8:\text{Dy}^{3+}$ (2.0 %) phosphor. The composition of the powder sample has been measured using an EDS spectrum. Table 2 shows the compositional (quantitative analysis) elements of $\text{BaAl}_2\text{Si}_2\text{O}_8:\text{Dy}^{3+}$ (2.0 %) phosphor, which is compared with the standard elements. An EDS is a standard procedure for identifying and quantifying elemental (chemical) composition of phosphors area, as small as a few nanometers. The elements appear in ratios concomitant with the proportions mixed in the starting materials, which represent the composition of the powder sample.

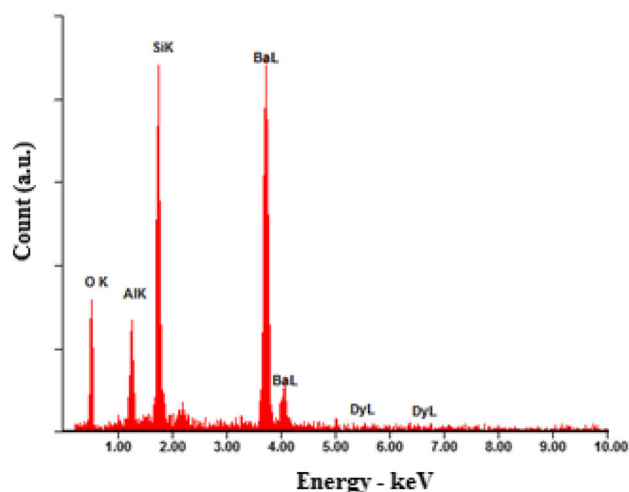


Fig. 5 EDS spectra of $\text{BaAl}_2\text{Si}_2\text{O}_8:\text{Dy}^{3+}$ (2.0 %) phosphor

Table 2 Chemical composition of $\text{BaAl}_2\text{Si}_2\text{O}_8:\text{Dy}^{3+}$ (2.0 %) phosphor

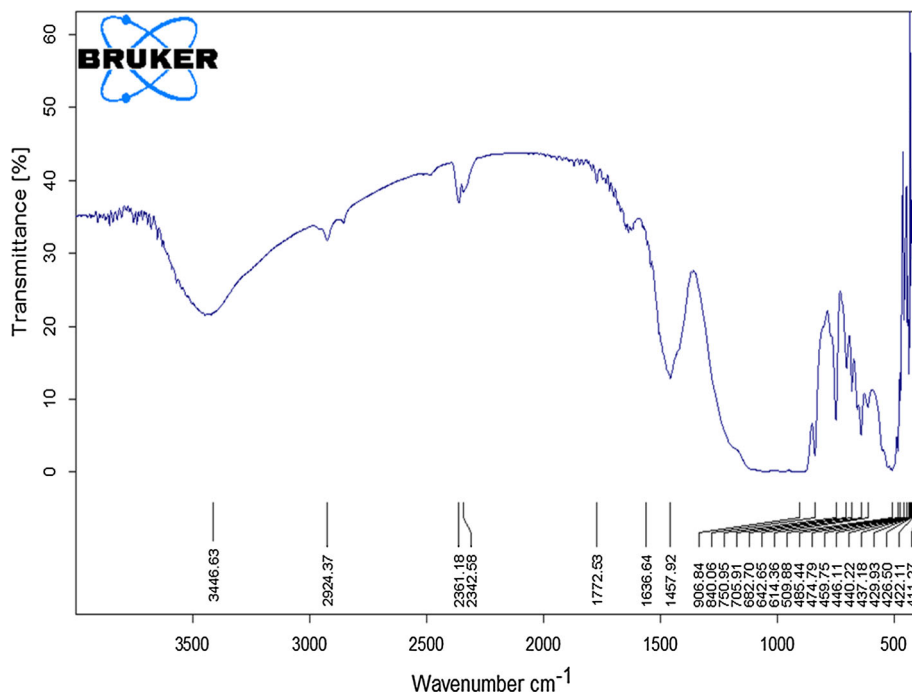
Sr. N.	Standard	Elements	Atomic (%)	Weight (%)
1	SiO_2	O K	43.18	55.02
2	Al_2O_3	Al K	18.93	16.45
3	SiO_2	Si K	18.37	15.19
4	BaF_2	Ba L	14.62	12.03
5	DyF_3	Dy L	4.89	1.30
Total			99.99	99.99

The existence of dysprosium (Dy) in prepared $\text{BaAl}_2\text{Si}_2\text{O}_8:\text{Dy}^{3+}$ (2.0 %) phosphor was clear in EDS spectra. Their appeared no other emissions apart from barium (Ba), aluminium (Al), silicon (Si) and oxygen (O) in the EDS spectra of the phosphor. In the EDS spectrum intense peaks are present which confirm the presence of elements in $\text{BaAl}_2\text{Si}_2\text{O}_8:\text{Dy}^{3+}$ (2.0 %) phosphor in Fig. 5. The elements appear in ratios concomitant with the proportions mixed in the starting materials, which is representing the composition of the powder sample.

3.5 Fourier transform infrared (FTIR) spectra

Figure 6 shows the FTIR spectra of $\text{BaAl}_2\text{Si}_2\text{O}_8:\text{Dy}^{3+}$ (2.0 %) phosphor. FTIR has been widely used for the identification of organic and inorganic compounds. The infrared spectrum of an organic and inorganic compound represents its physical properties. Spectroscopically, the middle infrared region ($4000\text{--}400\text{ cm}^{-1}$) is extremely useful for the study of organic and inorganic compounds. The FTIR spectrum of $\text{BaAl}_2\text{Si}_2\text{O}_8:\text{Dy}^{3+}$ (2.0 %) phosphor contains clearly exhibited bands in the region (3446.63 cm^{-1}) of hydroxyl group show the stretching vibration of hydroxyl (O–H) groups. The hydroxyl group in

Fig. 6 FTIR Spectra of $\text{BaAl}_2\text{Si}_2\text{O}_8:\text{Dy}^{3+}$ (2.0 %) phosphor



sintered phosphor is might be due to presence of moisture through environment [18]. A small peak originated at 2924.37 cm^{-1} is assigned to filter contamination of the FTIR instrument. The bands centred at 2342.58 , 2316.18 and 1772.53 cm^{-1} are attributed to carbonation processes. The free CO_3^{2-} ion has a $D3h$ symmetry (trigonal planar) and its spectrum is dominated by the band (asymmetric stretching) at 1636.64 cm^{-1} . Dy^{3+} ions are expected to replace Ba^{2+} sites because the coordination number of the Ba^{2+} ion is eight and that for Al^{3+} and Si^{4+} ions is four. Dy^{3+} ions cannot easily incorporate the tetrahedral $[\text{AlO}_4]$ or $[\text{SiO}_4]$ symmetry, but can easily incorporate octahedral $[\text{BaO}_8]$ [19]. Another fact that supports that the ionic radius of Dy^{3+} (0.99 \AA) are close to that of Ba^{2+} (about 1.42 \AA) rather than Al^{3+} (0.57 \AA) and Si^{4+} (0.41 \AA). Therefore, the Dy^{3+} ions are expected to occupy the Ba^{2+} sites in the $\text{BaAl}_2\text{Si}_2\text{O}_8:\text{Dy}^{3+}$ (2.0 %) phosphor. This might create distortion in the crystal lattice resulting in 1457.92 cm^{-1} vibration modes assigned to vibration in Ba^{2+} ions [20].

In the presented spectrum the absorption bands of aluminates and silicate groups were clearly evident. In the finger print region several bands are typical metal oxygen absorptions O–Al–O, Al–O, Ba–O, Sr–O, Si–O–Si and Si–O stretching frequencies were found [21]. The Si–O–Si and Si–O stretching modes for the silicate tetrahedral show infrared absorption bands, located at about 906.84 , 840.06 and 750.95 cm^{-1} . The bands at 682.7 , 642.65 and 614.36 cm^{-1} may be attributed to the Si–O symmetric stretch and Ba–O bending vibrations. The symmetric bonding of O–Al–O/Al–O appeared at 509.88 , 485.44 ,

474.79 , 459.75 , 446.11 , and 440.22 cm^{-1} . The anti-symmetric stretching bands 437.18 , 429.33 , 426.50 , 422.11 and 411.27 cm^{-1} are attributed due to the Sr–O vibrations.

3.6 Thermoluminescence (TL)

In order to study the trap states of the prepared $\text{BaAl}_2\text{Si}_2\text{O}_8:\text{Dy}^{3+}$ phosphors, TL glow curves were measured and are shown in Fig. 7. The phosphors were first irradiated for 10 min using 365 nm UV source, then the radiation source was removed and the irradiated samples were heated at a linear heating rate of $5\text{ }^\circ\text{C s}^{-1}$, from room temperatures to $300\text{ }^\circ\text{C}$. Initially the TL intensity increases with temperature, attains a peak value for a particular temperature and then it decreases with further increase in temperature. A

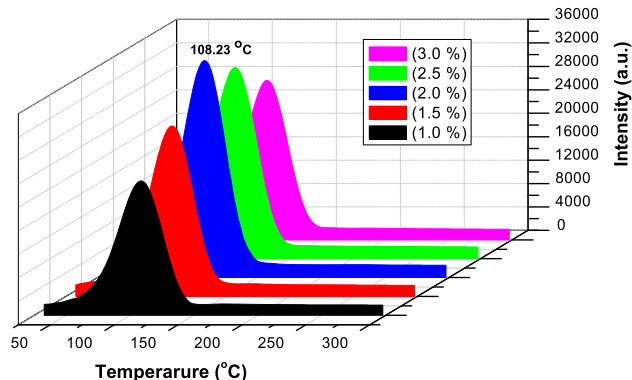


Fig. 7 Comparative TL glow curve of $\text{BaAl}_2\text{Si}_2\text{O}_8:\text{Dy}^{3+}$ phosphors with different Dy^{3+} concentration at 10 min UV irradiation

single glow peak of $\text{BaAl}_2\text{Si}_2\text{O}_8:\text{x}\text{Dy}^{3+}$ phosphors were obtained at 108.23 °C. The single isolated peak due to the formation of only one type of luminescence center which is created due to the UV irradiation. It is suggested that the recombination center associated with the glow at the temperature interval arises from the presence of liberated pairs, which are probably the results from the thermal release of electron/holes from different kinds of traps and recombine at the color centers. It is also known that the doping of the rare earth ions increases the lattice defects which have existed already in the host. The different TL parameters calculations are listed in Table 3.

3.6.1 Determination of kinetic parameters

Thermally stimulated luminescence is one of the most studied subjects in the field of condensed matter physics and a complete description of the thermoluminescent characteristics of a TL material requires obtaining these parameters. There are various methods for evaluating the trapping parameters [i.e. activation energy (E), order of kinetics (b) and frequency factor (s),] from TL glow curves [22]. For example, when one of the glow peaks is highly isolated from the others, the experimental method such as peak shape method is a suitable method to determine them from the glow peak. TL parameters of prepared phosphors were calculated using the peak shape method and shown in Table 3. The relationship between the frequency factor 's' and the activation energy 'E' is given by the Eq. (1)

$$\frac{\beta E}{kT_m^2} = s \left[1 + (b-1) \frac{2kT_m}{E} \right] \exp(E/KT_m) \quad (1)$$

where, k is Boltzmann constant, E is activation energy, b is order of kinetics, T_m is temperature of peak position, and β is the heating rate. In the present work $\beta = 5 \text{ }^\circ\text{C s}^{-1}$. Trap depth for second order kinetics is calculated using the Eq. (2)

$$E = 2kT_m \left(1.76 \frac{T_m}{\omega} - 1 \right) \quad (2)$$

where, ω is the total half width intensity $\omega = \tau + \delta$, τ is the half width at the low temperature side of the peak

($\tau = T_m - T_1$); δ is the half width towards the fall-off side of the glow peak ($\delta = T_2 - T_m$), and T_m is the peak temperature at the maximum. Chen provides a method which can identify the kinetics order for a model of one trap according to the shape of the TL band. The method involves the parameter $\mu_g (\mu_g = \delta/\omega)$. The shape factor (μ_g) is to differentiate between first and second order TL glow peak. ($\mu_g = 0.39 - 0.42$) for the first order kinetics, ($\mu_g = 0.42 - 0.48$) for the non-first order kinetics (mixed order) and ($\mu_g = 0.49 - 0.52$) for the second order kinetics [23]. In our case, shape factor (μ_g) is lies (as shown in Table 3) between 0.46 and 0.48, which indicates that it is a case of non-first order kinetics, approaching towards second order, responsible for deeper trap depth.

3.7 Photoluminescence (PL)

In order to study the photo-luminescent properties of phosphors, the excitation spectra of prepared $\text{BaAl}_2\text{Si}_2\text{O}_8:\text{x}\text{Dy}^{3+}$ phosphors were recorded and shown in Fig. 8a. The excitation spectra were observed in the range of 220–400 nm and emission spectra was recorded in the range of 400–700 nm. The excitation spectrum in the range of 220–400 nm consists of the $f \rightarrow f$ transition of the Dy^{3+} ion. The excitation spectrum of $\text{BaAl}_2\text{Si}_2\text{O}_8:\text{x}\text{Dy}^{3+}$ phosphor shows strong intense peak at 350 nm and less intense at 325, 338, 365 and 388 nm, which are ascribed to the transitions from the ground state to excitation states in the $4f^9$ configuration of Dy^{3+} but not easy to be clearly assigned due to the dense and somewhat overlapped levels of $4f$ configuration of Dy^{3+} in the high energy region. When the $\text{BaAl}_2\text{Si}_2\text{O}_8:\text{x}\text{Dy}^{3+}$ phosphors were excited at 350 nm, simultaneous emissions of blue (478 nm) and yellow (575 nm) position were observed. Notice that the blue emission is less intense than the yellow emissions. These two different emission bands originated from the one origin owing to their having the same excitation wavelength. The transitions involved in blue and yellow bands of Dy^{3+} ion are well known and have been identified as $^4\text{F}_{9/2} \rightarrow ^6\text{H}_{15/2}$, and $^4\text{F}_{9/2} \rightarrow ^6\text{H}_{13/2}$ transitions respectively. One can also find that the emission lines of Dy^{3+} are

Table 3 Activation energy (E), shape factor (μ_g) and frequency factor (s) for 10 min UV irradiated $\text{BaAl}_2\text{Si}_2\text{O}_8:\text{Dy}^{3+}$ phosphors for different Dy^{3+} concentration

Phosphors name	UV min	HTR	T_1 (°C)	T_m (°C)	T_2 (°C)	τ (°C)	δ (°C)	ω (°C)	$\mu_g = \delta/\omega$	Activation energy (eV)	Frequency factor
$\text{BaAl}_2\text{Si}_2\text{O}_8:\text{Dy}^{3+}$ (1.0 %)	10	5	86.49	108.23	128.20	21.74	19.97	41.71	0.48	0.99	6.70×10^{12}
$\text{BaAl}_2\text{Si}_2\text{O}_8:\text{Dy}^{3+}$ (1.5 %)	10	5	86.20	108.23	127.45	22.03	19.22	41.25	0.47	1.00	9.71×10^{12}
$\text{BaAl}_2\text{Si}_2\text{O}_8:\text{Dy}^{3+}$ (2.0 %)	10	5	87.39	108.23	127.80	20.84	19.57	40.41	0.48	1.02	1.95×10^{13}
$\text{BaAl}_2\text{Si}_2\text{O}_8:\text{Dy}^{3+}$ (2.5 %)	10	5	85.49	108.23	127.61	22.74	19.38	42.12	0.46	0.98	4.85×10^{12}
$\text{BaAl}_2\text{Si}_2\text{O}_8:\text{Dy}^{3+}$ (3.0 %)	10	5	85.51	108.23	127.68	22.72	19.45	42.17	0.46	0.97	4.66×10^{12}

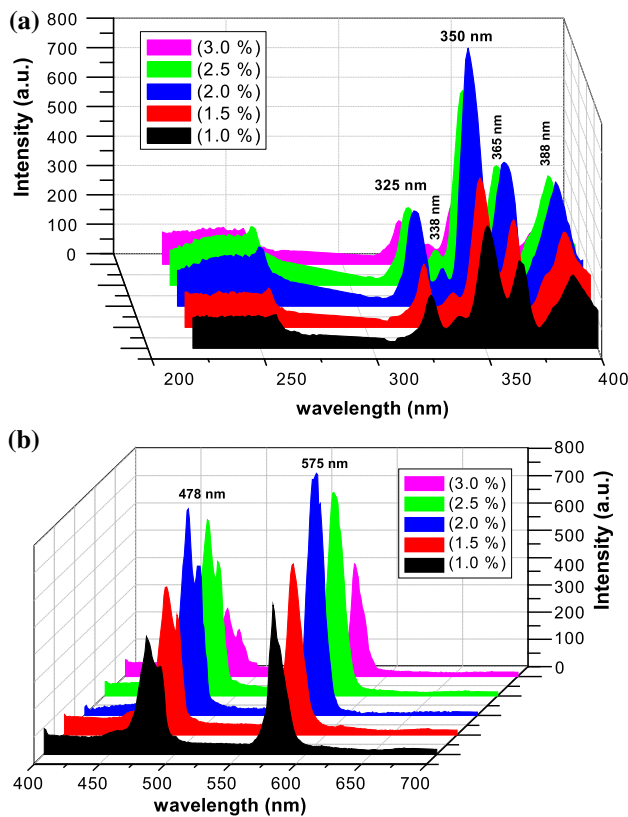
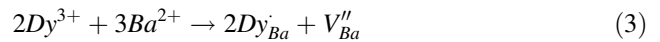


Fig. 8 **a** Excitation spectra of BaAl₂Si₂O₈:Dy³⁺ phosphors with different Dy³⁺ concentration. **b** Emission spectra of BaAl₂Si₂O₈:Dy³⁺ phosphors with different Dy³⁺ concentration

broadened somewhat because there are several Stark levels for the ⁴F_{9/2} → ⁶H_J levels [24].

Figure 8b shows that the emission spectra of BaAl₂Si₂O₈:x Dy³⁺ phosphors with different Dy³⁺ concentration. It is well known that the former weak blue emission at 478 nm (⁴F_{9/2} → ⁶H_{15/2}) is corresponded to the magnetic dipole transition, which hardly varies with the crystal field strength around Dy³⁺. While the later stronger yellow emission at 575 nm (⁴F_{9/2} → ⁶H_{13/2}) belongs to the hypersensitive forced electric dipole transition, which is strongly influenced by the outside surrounding environment [25]. According to the Judd–Ofelt theory [26], when Dy³⁺ locates at a low symmetry local site (without inversion symmetry), a yellow emission according to the electric dipole transition (⁴F_{9/2} → ⁶H_{13/2}) will be dominant. Conversely, a magnetic dipole transition (⁴F_{9/2} → ⁶H_{15/2}) will predominate in the emission spectra, resulting in a strong blue emission. In our case, the yellow emission (⁴F_{9/2} → ⁶H_{13/2}) will dominate. The strong yellow emission is also beneficial to decrease the color temperature of the phosphor and generate warm white light emission. The optical properties of the material are often influenced by the structure of the matrix and synthesis technique [27].

When trivalent rare earth ions such as Dy³⁺ are incorporated into a host lattice and substitute divalent metallic ions Ba²⁺, the charge balancing is necessarily required. Due to these chemically nonequivalent substitutions, an excess of positive charge in the host lattice must be compensated [28]. One possible way of charge compensation mechanism is that two Dy³⁺ ions replace three Ba²⁺ ions to balance the charge of these phosphors, which create two Dy_{Ba}⁺ positive defects and one V_{Ba}^{''} negative defect.



For BaAl₂Si₂O₈:xDy³⁺ phosphors, the incorporation of alkali metal ions can neutralize the charge generated by Dy³⁺ substitution for Ba²⁺, and thus stabilize the structure and enhance the luminescence. Dy³⁺ ions have been often used as co-dopants in the previously developed aluminate and silicate based materials. When divalent alkaline earth ions, such as Ca²⁺ or Sr²⁺ or Ba²⁺ is substituted by trivalent Dy³⁺ in the alkaline earth silicates and aluminates, various defects can be induced due to the charge compensation mechanism. However, in Dy³⁺ singly doped samples, which are in our current interest, Dy³⁺ is not only the supplier of traps but also an activator itself [29]. The energy level diagram of Dy³⁺ ions were shown in Fig. 9a.

A schematic process of emitting the white light in BaAl₂Si₂O₈:xDy³⁺ phosphors were illustrated schematically in Fig. 9b. After irradiation with the ultraviolet light (process numbered [1]), most of the excitation energy associated with the excited carriers (electrons or holes) will be transferred via the host directly to the luminescence centers, Dy³⁺, followed by the Dy³⁺ 4f emissions as the immediate luminescence (process [2]). However, part of the excitation energy will be stored when some of the excited carriers drop into the traps (process [3]), instead of returning to the ground states. Later, with thermal excitation at proper temperature, these carriers will be released from the traps and transferred via the host to the Dy³⁺ ions, followed by the characteristic Dy³⁺ emissions as long afterglow (process [4]). In the practical system, the electron traps and the hole traps may not be both equally abundant or important in terms of their contribution to the white light emission, as suggested in Fig. 9b.

To investigate the concentration dependent luminescent property of Dy³⁺ ions doped BaAl₂Si₂O₈ host, a series of BaAl₂Si₂O₈:xDy³⁺ (x = 1.0, 1.5, 2.0, 2.5 and 3.0 %) phosphors were synthesized and the luminescent properties were measured are shown in Fig. 8b. It can be seen that all the emission spectra are similar regardless of Dy³⁺ contents. In BaAl₂Si₂O₈ host, the Dy³⁺ impurity concentration were increased in the range from 1.0–3.0 mol% and the maximum emission intensity was observed at 2.0 mol%. Dy³⁺ concentration (x) dependence of the emission intensities is shown in the Fig. 8b. The concentration quenching

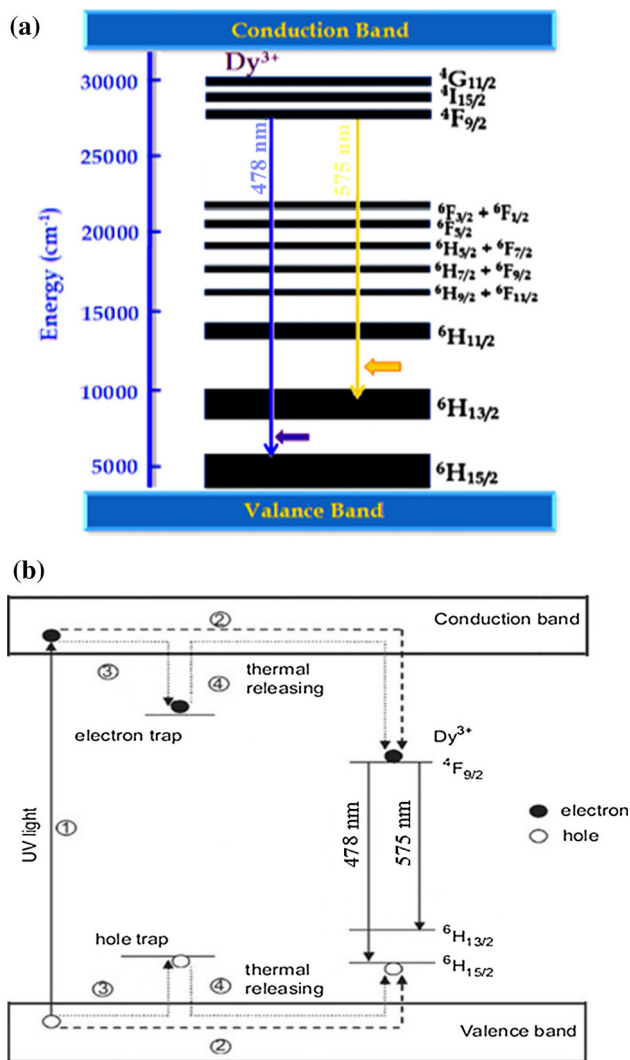


Fig. 9 **a** Energy level diagram of Dy³⁺ ions. **b** Schematic process of white light emission in BaAl₂Si₂O₈:xDy³⁺ phosphors

was observed for higher doping concentration of Dy³⁺. If there is an increase in concentration of the lanthanide ions in a given material it should be accompanied by an increase in the emitted light intensity, but it has been established that such behavior occurs up to a certain critical concentration. Above this critical concentration the luminescence intensity starts to decrease. This process is known as concentration quenching of the luminescence. The concentration quenching is due to energy transfer from one activator (donor) to another until the energy sink (acceptor) in the lattice is reached. Hence, the energy transfer will strongly depend on the distance (R_c) between the Eu³⁺ ions, which can be obtained using the following Eq. (4) [30].

$$R_c \approx 2 \left[\frac{3V}{4\pi X_c Z} \right]^{\frac{1}{3}} \quad (4)$$

where X_c is the critical concentration, Z is the number of cation sites in the BaAl₂Si₂O₈ unit cell [$Z = 1$ in BaAl₂Si₂O₈], and V is the volume of the unit cell ($V = 187.00$ (Å)³ in this case). The critical concentration is estimated to be about $x = 2.0$ mol%, where the measured emission intensity begin to decrease. The critical distance (R_c) between the donor and acceptor can be calculated from the critical concentration, for which the nonradiative transfer rate equals the internal decay rate (radiative rate). Blasse [31] assumed that, for the critical concentration, the average shortest distance between the nearest activator ions is equal to the critical distance. By taking the experimental and analytic values of V , Z and X_c (187.00 (Å)³, 1, 2.0 mol%, respectively), the critical distance R_c is estimated by Eq. (1) is equal to 22.83 Å in this host. The value of R_c is greater than 5 Å for the rare earth ions indicating that the multipole–multipole interaction is dominant and is the major cause of concentration quenching of Dy³⁺ in the phosphors.

3.8 CIE chromaticity coordinate

In general, color coordinates are one of the important factors for evaluating phosphors color. The luminescence color of the samples excited under 350 nm has been characterized by the CIE (Commission International de l'Éclairage) 1931 chromaticity diagram. The emission spectrum of the BaAl₂Si₂O₈:Dy³⁺ (2.0 %) phosphor was converted to the CIE 1931 chromaticity using the photoluminescent data and the interactive CIE software (CIE coordinate calculator) [32] diagram as shown in Fig. 10.

Every natural color can be identified by (x , y) coordinates that are disposed inside the ‘chromatic shoe’ representing the saturated colors. Luminescence colors of BaAl₂Si₂O₈:Dy³⁺ (2.0 %) phosphor are placed in ($x = 0.3310$, $y = 0.3600$), which is represented by the circle symbol [“o”]. It indicates that the color coordinates of BaAl₂Si₂O₈:Dy³⁺ (2.0 %) phosphors were very close to the “ideal white light emission” ($x = 0.3333$, $y = 0.3333$) in chromaticity diagram. The other prepared BaAl₂Si₂O₈:xDy³⁺ ($x = 1.0$, 1.5, 2.5 and 3.0 %) phosphors were also placed in ($x = 0.3170$, $y = 0.3280$); ($x = 0.3210$, $y = 0.3450$); ($x = 0.3090$, $y = 0.3280$) and ($x = 0.3100$, $y = 0.3230$) corners [Inset Fig. 10; Table 4]. The chromatic co-ordinates of the luminescence of this phosphor are measure and reached to near white light emission [33].

The chromaticity diagram of the CIE indicates that coordinates are highly useful in determining the exact emission color and color purity of a sample. Because the color purity is considered as one of the important factors for evaluating the performance of phosphors, the color

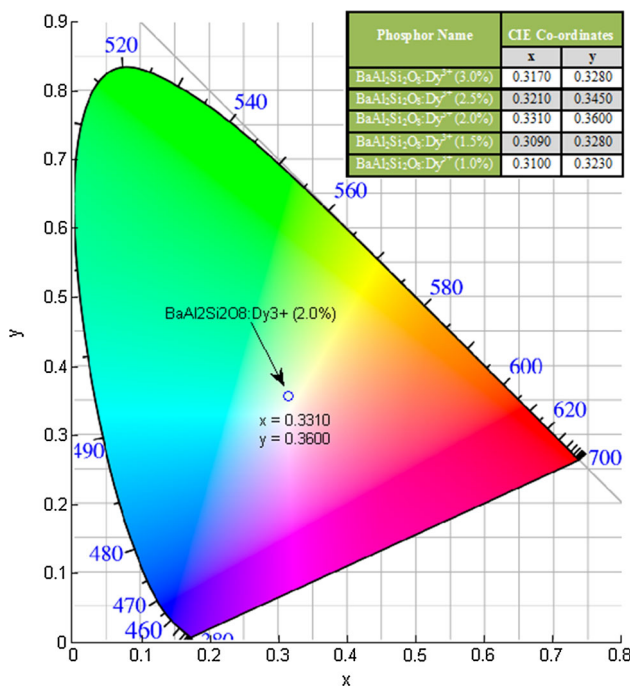


Fig. 10 CIE chromaticity diagram of BaAl₂Si₂O₈:Dy³⁺ (2.0%) phosphor

purity of samples has been calculated by the following Eq. (5) [34]:

$$\text{Color purity} = \frac{\sqrt{(x - x_i)^2 + (y - y_i)^2}}{\sqrt{(x_d - x_i)^2 + (y_d - x_i)^2}} \cdot 100\% \quad (5)$$

where (x, y) and (x_i, y_i) are the color coordinates of the light source and the CIE equal-energy illuminant respectively; (x_d, y_d) is the chromaticity coordinate corresponding to the dominant wavelength of light source. For BaAl₂Si₂O₈:x Dy³⁺ (x = 1.0, 1.5, 2.0, 2.5 and 3.0 %) phosphors, and the coordinates of (x, y) are (x = 0.3170, y = 0.3280); (x = 0.3210, y = 0.3450); (x = 0.3310, y = 0.3600); (x = 0.3090, y = 0.3280) and (x = 0.3100, y = 0.3230) respectively; the coordinates of (x_i, y_i) is (0.3333, 0.3333); (x_b, y_d) is (0.3160, 0.3270); (x = 0.3202, y = 0.3447); (x = 0.3307, y = 0.3598); (x = 0.3083, y = 0.3277) and (x = 0.3090, y = 0.3200) corresponding to the dominant wavelength 575 nm. Based on these coordinate values and

Table 4 CCT, CRI and color purity calculation of BaAl₂Si₂O₈:Dy³⁺ phosphors for different Dy³⁺ concentration

Sr. no.	Phosphors name	CIE chromaticity co-ordinates		CCT (K)	CRI	Color purity
		x	y			
1	BaAl ₂ Si ₂ O ₈ :Dy ³⁺ (1.0 %)	0.3170	0.3280	6280	65.53	93.09 %
2	BaAl ₂ Si ₂ O ₈ :Dy ³⁺ (1.5 %)	0.3210	0.3450	6008	66.81	97.75 %
3	BaAl ₂ Si ₂ O ₈ :Dy ³⁺ (2.0 %)	0.3310	0.3600	5559	67.07	100.00 %
4	BaAl ₂ Si ₂ O ₈ :Dy ³⁺ (2.5 %)	0.3090	0.3280	6719	64.84	97.07 %
5	BaAl ₂ Si ₂ O ₈ :Dy ³⁺ (3.0 %)	0.3100	0.3230	6708	62.76	95.06 %

Eq. (4), we finally get the color purity of BaAl₂Si₂O₈:x Dy³⁺ (x = 1.0, 1.5, 2.0, 2.5 and 3.0 %) phosphors as 93.09, 97.75, 100.00, 97.07 and 95.06 % respectively. It is worthwhile to mention that the CIE chromaticity coordinate of BaAl₂Si₂O₈:x Dy³⁺ phosphors are very close to those corresponding dominant wavelength points, and that almost pure white color purity phosphors have been obtained in our work.

3.9 Correlated color temperature (CCT)

CCT relates to the color of light produced by a light source, measured in degrees Kelvin. The CCT rating is an indication of how “warm” or “cool” the light source appears. The higher the CCT value, the cooler the lamp color will appear. The lower the number, the warmer the lamp color will appear. However, CCT is only one aspect of color. However, opposite to the temperature scale, lamps with a CCT rating below 3200 K are usually considered “warm” sources, while those with a CCT above 4000 K are usually considered “cool” in appearance. McCamy has proposed the analytical Eq. (6) to calculate the CCT which is given [35] by

$$CCT = -449n^3 + 3525n^2 - 6823n + 5520.33 \quad (6)$$

where, n = (x - x_e)/(y - y_e) is the inverse slope line and (x_e = 0.332, y_e = 0.186) is the epicenter. Generally, the preferred CCT values range from 4000 to 6500 K but the range from 3500 to 7500 K may also be accepted. The calculated CCT values of prepare BaAl₂Si₂O₈:x Dy³⁺ (x = 1.0, 1.5, 2.0, 2.5 and 3.0 %) phosphors were 6280, 6008, 5559, 6719 and 6708 K respectively, which is well under the acceptable ranged and can be considered “cool” in appearance [36].

3.10 Color rendering index (CRI)

The CRI, sometimes called color rendition index, is a quantitative measurement of the ability of a light source to reveal the colors of various objects faithfully in comparison with an ideal or natural light source. The ability of any given light source to represent colors in objects is its CRI. It is based on a relative measurement which will rate light

sources on a scale of 0–100 [37]. The higher the CRI, the more natural the colors appear. A higher CRI means better color rendering, or less color shift. CRIs in the range of 75–100 are considered excellent, while 65–75 are good. The range of 55–65 is fair, and 0–55 is poor [38]. Under higher CRI sources, surface colors appear brighter, improving the aesthetics of the space. Sometimes, higher CRI sources create the illusion of higher illuminance levels. The values of CRI were also calculated and listed in Table 4. The calculated CRI of prepared $\text{BaAl}_2\text{Si}_2\text{O}_8:\text{Dy}^{3+}$ (2.0 %) phosphors were 65.53, 66.81, 67.07, 64.84 and 62.76 respectively, which is again in the preferable range. CRI of different samples varies from 62.76 to 67.07, which is again well under the preferable range.

3.11 Decay

Figure 11 shows the typical decay curves of $\text{BaAl}_2\text{Si}_2\text{O}_8:\text{Dy}^{3+}$ (2.0 %) phosphor. The initial afterglow intensity of the sintered $\text{BaAl}_2\text{Si}_2\text{O}_8:\text{Dy}^{3+}$ (2.0 %) phosphor was high. The decay times of phosphor can be calculated by a curve fitting technique, and decay curves fitted by the sum of two exponential components have different decay times.

$$I = A_1 \exp(-t/\tau_1) + A_2 \exp(-t/\tau_2) \quad (7)$$

where, I is phosphorescence intensity, A_1, A_2 are constants, t is time, τ_1 and τ_2 are decay times (in microsecond) for the exponential components. Decay curves are successfully fitted by the Eq. (7) and the fitting curve result are shown in inset of Fig. 11 with the standard error. The results indicated that the prepared $\text{BaAl}_2\text{Si}_2\text{O}_8:\text{Dy}^{3+}$ (2.0 %) phosphor shows a rapid decay and the subsequent slow decaying process [39].

Dy^{3+} is an important rare earth ion in the development of phosphors with long lasting afterglow, playing a crucial role. The dopant Dy^{3+} is a famous trap creating ion, which can greatly prolong the afterglow. It is reasonable to

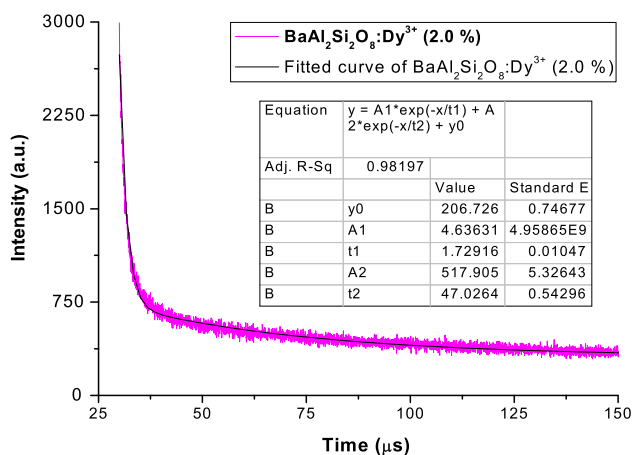


Fig. 11 Decay curves of $\text{BaAl}_2\text{Si}_2\text{O}_8:\text{Dy}^{3+}$ (2.0 %) phosphor

consider that the role of doping Dy^{3+} ions is to introduce new types of traps or significantly increase the concentration of traps responsible for the afterglow. The afterglow intensity of the persistent phosphor depends on the densities of the traps electrons, while the duration of afterglow depends on the depth of the trapped electrons. The number of trapped charge carrier, in term, depends on the concentration of oxygen vacancies/ Dy^{3+} and the trap depth of it. For a suitable trap depth, the trap concentration is directly depends on the dysprosium ions [40].

3.12 Mechanoluminescence (ML)

Mechanoluminescence (ML) is an important physical phenomenon where an emission of light is observed due to mechanical deformation of materials like rubbing, cleavage, compressing, impulsive deformation, crushing, grinding, shaking etc. In the present ML studies, an impulsive deformation technique has been used. When a moving piston was applied on to the phosphor, initially the ML intensity increases with time, attains a peak value and then decreases with time. Such a curve between the ML intensity and deformation time of phosphors is known as the ML glow curve [41].

Figure 12 shows that the characteristics curve between ML intensity versus time for different heights ($h = 10, 20, 30, 40, 50$ cm). The phosphor was fracture via dropping a load [moving piston] of particular mass (400 g) and cylindrical shape on the $\text{BaAl}_2\text{Si}_2\text{O}_8:\text{Dy}^{3+}$ (2.0 %) phosphor. The velocity of the moving piston, holding the impact mass, could be changed, by changing the height through which it was dropped. Every time for the ML

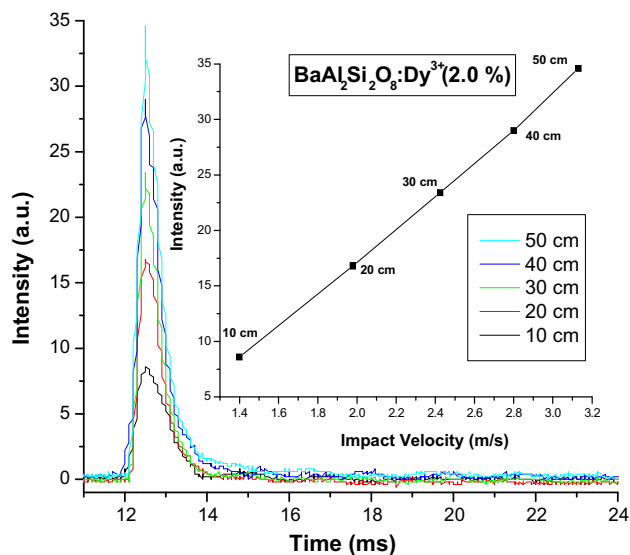


Fig. 12 ML intensity versus time curve of $\text{BaAl}_2\text{Si}_2\text{O}_8:\text{Dy}^{3+}$ (2.0 %) phosphor (inset ML intensity vs. impact velocity curve of $\text{BaAl}_2\text{Si}_2\text{O}_8:\text{Dy}^{3+}$ (2.0 %) phosphor)

measurement, the quantity of BaAl₂Si₂O₈:Dy³⁺ (2.0 %) phosphor was kept constant (8 mg). When the moving piston is dropped onto the prepared phosphor at different height, a great number of physical processes may occur within very short time intervals, which may excite or stimulate the process of photon emission and light is emitted. The photon emission time is nearly 2 ms, when prepared BaAl₂Si₂O₈:Dy³⁺ (2.0 %) phosphor fractures [42]. In these ML measurements, maximum ML intensity has been obtained for the 50 cm dropping height and ML intensity increases linearly with the increases the falling height of the moving piston. The sintered BaAl₂Si₂O₈:Dy³⁺ (2.0 %) phosphor was not irradiated by any excitation source.

Figure 12 (inset) shows the characteristics curve of ML intensity versus impact velocities for BaAl₂Si₂O₈:Dy³⁺ (2.0 %) phosphor. The ML intensity of BaAl₂Si₂O₈:Dy³⁺ (2.0 %) phosphor increases linearly with increasing the mechanical stress [43]. When the load or piston makes an impact on the crystal with an initial velocity v₀, the former decelerates and after a particular time its velocity becomes zero. The time dependence of the velocity of the piston may be written as

$$v = v_0 \exp(-\beta v_0 t) \tag{8}$$

where β is a constant, Eq. (8) can be written as

$$\frac{dx}{dt} = v_0 \exp(-\beta v_0 t) \tag{9}$$

where dx is the compression of the crystal during the time interval dt.

Integrating Eq. (10), we have

$$x = \frac{1}{\beta} \exp(-\beta v_0 t) + C \tag{10}$$

x = 0 for t = 0, therefore, Eq. (9) may be written as

$$x = \frac{1}{\beta} [1 - \exp(-\beta v_0 t)] \tag{11}$$

The phosphor is in powder form and the impact velocities compress it to a certain extent, but this does not change significantly with increasing impact velocity. Equation (10) shows that impact time remains mostly unchanged with increasing impact velocity because there is no significant change in compression, which is expressed by ‘x’ in Eq. (10). This may be one possible reason why the time that corresponds to the peak ML intensity does not change significantly with increasing impact velocity [44]. Figure 13 shows the time corresponds to ML signal peak with impact velocity of BaAl₂Si₂O₈:Dy³⁺ (2.0 %) phosphor.

The relationship between semi-log plot of ML intensity versus (t – t_m) for BaAl₂Si₂O₈:Dy³⁺ (2.0 %) phosphor is

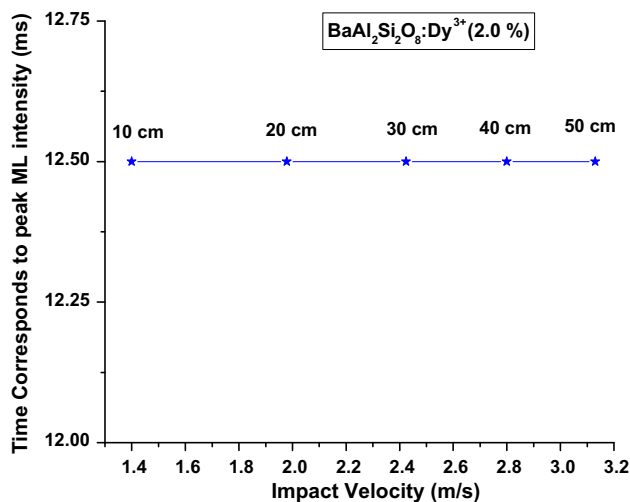


Fig. 13 Time corresponds to ML signal peak with impact velocity of BaAl₂Si₂O₈:Dy³⁺ (2.0 %) phosphor

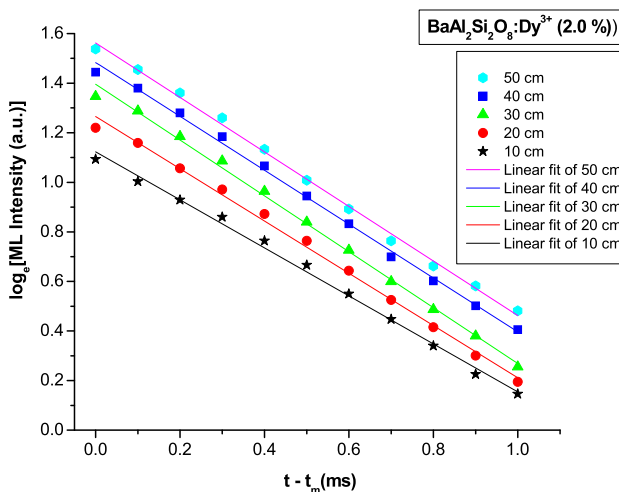


Fig. 14 Semi-log plot of ML intensity versus (t – t_m) for BaAl₂Si₂O₈:Dy³⁺ (2.0 %) phosphor

shown in Fig. 14, and the lines were fitted using the following Eq. (12) with Origin 8.0

$$\tau = \frac{1}{\text{slope of straight line}} \tag{12}$$

Curve fitting results show that decay constant (τ) varies from 0.89 to 1.04 ms. The ML decay constant value is maximum for the low impact velocities (Table 5). Decay

Table 5 Calculation of ML decay constant for BaAl₂Si₂O₈:Dy³⁺ (2.0 %) phosphor

Impact velocity	10 cm	20 cm	30 cm	40 cm	50 cm
τ decay constant (ms)	1.04	0.95	0.89	0.92	0.91
Standard error (ms)	0.02	0.02	0.02	0.01	0.01

rates of the exponentially decaying period of the ML curves did not change significantly with impact velocity. In order to further clarification of the ML decay mechanism in $\text{BaAl}_2\text{Si}_2\text{O}_8:\text{Dy}^{3+}$ (2.0 %) phosphor, more experimental and theoretical studies are needed.

When a mechanical stress, such as compress, friction, and striking, and so on, was applied onto the sintered $\text{BaAl}_2\text{Si}_2\text{O}_8:\text{Dy}^{3+}$ (2.0 %) phosphor, local piezoelectric field can be produced. Therefore, in such phosphor the ML excitation may be caused by the local piezoelectric field near the impurities and defects in the crystals. During the impact on the material, one of its newly created surfaces gets positively charged and the other surface of the crack gets negatively charged (Fig. 15). Thus, an intense electric field in the order of 10^6 – 10^7 V cm^{-1} is produced [45]. Under such order of electric field, the ejected electrons from the negatively charged surface may be accelerated and subsequently their impact on the positively charged surfaces may excite the luminescence center. Subsequently, the de-excitation of excited Dy^{3+} ions may give rise to the light emission due to the transition from ${}^4\text{F}_{9/2}$ state to ${}^6\text{H}_{15/2}$ and ${}^6\text{H}_{13/2}$ respectively, emitting radiation at 478 and 575 nm. As the height of the piston increases the area of newly created surface increases, hence free electrons and holes were generated and the subsequent recombination of electrons/hole with the electron/holes trap centers gave rise to the light emission.

With the increasing impact velocity, more compression of the sample takes place, and therefore, more area of the newly created surface takes place. Thus, the ML intensity will increase with increasing value of the impact velocity. It is to be noted that the stress near the tip of a moving crack is of the order of $Y/100 \approx 10^{10}$ dyn $\text{cm}^{-2} = 10^9$ N m^{-2} (where Y is the Young's modulus of the materials). Thus, a fixed charge density will be produced on the newly created surfaces and the increase in the ML intensity will primarily be caused by the increase in the rate of newly

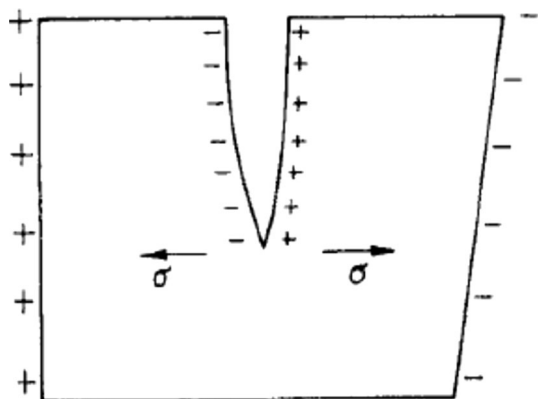


Fig. 15 Langevin model for the piezo-electrification induce phosphor

created surface area with increasing impact velocity [46]. Moreover, the total ML intensity will also increase with impact velocity because more compression of the sample will create more surfaces with increasing impact velocity. As the impact velocity increases, the impact pressure also increases leading to the increase in the electric field at local region which causes the decrease in trap depth. Hence the probability of de-trapping increases. From Fig. 12 (inset), it can be seen that with increasing impact velocity, ML intensity also increases linearly i.e., the ML intensity of $\text{BaAl}_2\text{Si}_2\text{O}_8:\text{Dy}^{3+}$ (2.0 %) phosphor are lineally proportional to the magnitude of the impact velocity, which suggests that this phosphor can be used as sensors to detect the stress of an object [47].

4 Conclusion

In summary, $\text{BaAl}_2\text{Si}_2\text{O}_8:\text{xDy}^{3+}$ phosphors were prepared by the traditional high temperature solid state reaction method. The hexagonal structure of prepared $\text{BaAl}_2\text{Si}_2\text{O}_8:\text{xDy}^{3+}$ phosphors were confirmed by the XRD. TL, and PL intensity increases with increase concentration of Dy^{3+} ions. It reaches optimum intensity when concentration of Dy^{3+} ions was 2.0 mol%, then TL and PL intensity decrease due to concentration quenching of Dy^{3+} ions. The life time of $\text{BaAl}_2\text{Si}_2\text{O}_8:\text{Dy}^{3+}$ (2.0 %) phosphor can be calculated by a curve fitting technique, and the decay curves fitted by the sum of two exponential components have different decay times ($\tau_1 = 1.72$ μs ; $\tau_2 = 47.02$ μs) and they possess the fast and slow decay process. CIE color chromaticity diagram, PL spectra, color purity, CCT and CRI indicating that it has the white light emission and excellent color stability properties for the WLED application. It is worthy to note that the dependence ML intensity to the impact velocity is close to linearity, which suggests that, $\text{BaAl}_2\text{Si}_2\text{O}_8:\text{Dy}^{3+}$ (2.0 %) phosphor can be used as sensors to detect the stress of an object. The time of the peak ML and the rate of decay did not change significantly with respect to increasing impact velocity of the moving piston.

References

1. T. Justela, J. Krupab, D. Wiecherta, J. Lumin. **93**, 179–189 (2001)
2. L. Tian, B. Yu, C. Pyun, H. Park, S. Mho, J. Solid State Commun. **129**, 43–46 (2004)
3. L. Lin, C.S. Shi, Z.F. Wang, W.P. Zhang, M. Yin, J. Alloys Compd. **466**, 546–550 (2008)
4. Y. Liu, B. Lei, C. Shi, Chem. Mater. **17**, 2108–2113 (2005)
5. I.P. Sahu, P. Chandrakar, R.N. Baghel, D.P. Bisen, N. Brahme, R.K. Tamrakar, J. Alloys Compd. **649**, 1329–1338 (2015)

6. F. Clabau, A. Garcia, P. Bonville, D. Gonbeau, M.T. Le, P. Deniard, S. Jobic, J. Solid State Chem. **181**, 1456 (2008)
7. C. Zhang, J. Yang, C. Lin, C. Li, J. Lin, J. Solid State Chem. **182**, 1673 (2009)
8. S. Ye, Z.S. Liu, X.T. Wang, J.G. Wang, L.X. Wang, X.P. Jing, J. Lumin. **129**, 50 (2009)
9. C.Y. Shen, Y. Yang, S.Z. Jin, H.J. Feng, Optik **121**, 29 (2010)
10. M. Ma, D. Zhu, C. Zhao, T. Han, S. Cao, M. Tu, Opt. Commun. **285**, 665 (2012)
11. V.B. Pawade, S.J. Dhoble, J. Lumin. **145**, 626 (2014)
12. V.B. Pawade, N.S. Dhoble, S.J. Dhoble, J. Rare Earths **32**, 593 (2014)
13. L. Lia, X. Liua, H.M. Noh, B.K. Moon, B.C. Choi, J.H. Jeong, Ceram. Int. **41**, 9722 (2015)
14. I.P. Sahu, D.P. Bisen, N. Brahme, L. Wanjari, R.K. Tamrakar, Res. Chem. Intermed. **41**(11), 8797–8814 (2015)
15. I.P. Sahu, D.P. Bisen, N. Brahme, Lumin. J. Biol. Chem. Lumin. **30**(7), 1125–1132 (2015)
16. I.P. Sahu, D.P. Bisen, N. Brahme, J. Mater. Sci. Mater. Electron. **27**(4), 3934–3940 (2016)
17. JCPDS file number 24-1230, JCPDS International Center for Diffraction Data
18. M.A. Salim, R. Hussain, M.S. Abdullah, S. Abdullah, N.S. Alias, Solid State Sci. Technol. **17**, 59–64 (2009)
19. Z. Gou, J. Chang, W. Zhai, J. Eur. Ceram. Soc. **25**, 1507–1514 (2005)
20. I.P. Sahu, D.P. Bisen, N. Brahme, Displays **38**, 68–76 (2015)
21. G.T. Chandrappa, S. Ghosh, K.C. Patil, J. Mater. Syn. Process. **7**, 273–279 (1999)
22. J. Kuang, Y. Liu, J. Zhang, J. Solid State Chem. **179**, 266–269 (2006)
23. V. Pagonis, G. Kitis, C. Furetta, *Numerical and Practical Exercises in Thermoluminescence* (Springer, Berlin, 2006)
24. G.S. Rama Raju, J.Y. Park, H.C. Jung, B.K. Moon, J.H. Jeong, J.H. Kim, Curr. Appl Phys. **9**(2), 92–95 (2009)
25. Y. Chen, X. Cheng, M. Liu, Z. Qi, C. Shi, J. Lumine **129**, 531–535 (2009)
26. A. Zukauskas, M.S. Shur, R. Gaska, *Introduction to Solid State Lighting* (Wiley, New York, 2002)
27. B.M. Mothudi, O.M. Ntwaeaborwa, S.S. Pitale, H.C. Swart, J. Alloys Compd. **508**, 262–265 (2010)
28. B. Liu, Y. Wang, J. Zhou, F. Zhang, Z. Wang, J. Appl. Phys. **106**(5), 053102 (2009)
29. V.B. Rao, K.W. Jang, H.S. Lee, S.S. Yi, J.H. Jeong, J. Alloys Compd. **496**, 251–255 (2010)
30. G. Blasse, Philips Res. Rep. **24**, 131 (1969)
31. G. Blasse, B.C. Grabmarier, *Luminescent Materials*, vol. 96 (Springer, Berlin, 1994)
32. CIE (1931). International Commission on Illumination. Publication CIE No. 15 (E-1.3.1)
33. I.P. Sahu, D.P. Bisen, N. Brahme, R.K. Tamrakar, J. Mater. Sci. Mater. Electron. **27**(2), 1828–1839 (2016)
34. J. Suresh Kumar, K. Pavani, A. Mohan Babu, N. Kumar Giri, S.B. Rai, L.R. Moorthy, J. Lumin. **130**, 1916–1923 (2010)
35. C.S. McCamy, Color Res. Appl. **17**, 142 (1992)
36. Y. Chen, X. Cheng, M. Liu, Z. Qi, C. Shi, J. Lumine **129**, 531 (2009)
37. A. Zukauskas, M.S. Shur, R. Gaska, *Introduction to Solid State Lighting* (Wiley, New York, 2002)
38. R. Rajeswari, C.K. Jayasankar, D. Ramachari, S. Surendra Babu, Ceram. Int. **39**, 7523 (2013)
39. I.P. Sahu, D.P. Bisen, N. Brahme, R.K. Tamrakar, R. Shrivastava, J. Mater. Sci. Mater. Electron. **26**, 9907–9920 (2015)
40. K.V.D. Eeckhout, P.F. Smet, D. Poelman, Materials **3**, 2536–2566 (2010)
41. D.R. Vij, *Luminescence of Solids* (Plenum Press, New York, 1998)
42. I.P. Sahu, J. Mater. Sci. Mater. Electron. (2016). doi:[10.1007/s10854-016-4944-0](https://doi.org/10.1007/s10854-016-4944-0)
43. I.P. Sahu, J. Mater. Sci. Mater. Electron. **26**(9), 7059–7072 (2015)
44. I.P. Sahu, D.P. Bisen, N. Brahme, R.K. Tamrakar, J. Electron. Mater. **45**, 2222–2232 (2016)
45. B.P. Chandra, R.A. Rathore, Cryst. Res. Tech. **30**, 885–896 (1995)
46. I.P. Sahu, D.P. Bisen, N. Brahme, M. Ganjir, Lumin. J. Biol. Chem. Lumin. **30**(8), 1318–1325 (2015)
47. I.P. Sahu, D.P. Bisen, R.K. Tamrakar, R. Shrivastava, Res. Chem. Intermed. **42**, 1823–1843 (2016)